DFT study ofstructural, electronic, optical and electrical properties of CuObased on GGA+U and TB-mBJ approximations

Adil Es-Smairi[1], Nejma Fazouan[1,2], El Houssine Atmani[1], E. Maskar[3], Tuan V. Vu[4,5], D. P. Rai[4,5]*

[1]Laboratory of Physics of Condensed Matters and Renewables Energies, Hassan II University, Faculty of Sciences and Technologies, B.P 146, 20650 Mohammedia, Morocco.
[2]Laboratory of Materials Physics, Sulttan Moulay Slimane University, Faculty of Science anTechnologies, B.P 523, 23000 Beni Mellal, Morocco.
[3]Nanomaterial and Nanotechnology Unit. E. N. S. Rabat. Energy Research Center. Faculty of Sciences, Mohammed V University, B.P. 1014 Rabat, Morocco.
[4]Division of Computational Physics, Institute for Computational Science, Ton Duc Thang University, Ho Chi Minh City, Vietnam
[5]Faculty of Electrical and Electronics Engineering, Ton Duc Thang University, Ho Chi Minh City, Vietnam
Email*:dibya@tdtu.edu.vn

Abstract.

The structural, electronic, optical, and electrical properties of CuO were studied using the density functional theory (DFT) based on the Full Potential Linearized Augmented Plane Wave (FP-LAPW) method as implemented in the Wien2k code. The structural parameters are optimized by using the 4D-optimize option and the PBE-sol functional. The electronic and optical properties were analysed adopting Generalized Gradient approximation plus the screened Coulomb interaction (GGA+U) and the modified Becke-Johnson (GGA-TB-mBJ) potential for comparison. The calculated band energies have been used with the Boltzmann transport equation to calculate the thermoelectric properties. It is shown that the gap energy obtained by the (TB-mBJ) approximation potential is 2.02 eV more close to the experimental values comparing to that given by the GGA+U (Eg=1.57 eV). The optical properties reveal a high absorption coefficient in the UV region with an average transmittance of around 65% in the visible range, which covers a high range of light using TB-mBJ exchange potential and an average reflectivity of approximately 18% in visible light. The CuO conductivity is limited by the carrier mobility at low temperature and primarily defined by the carrier concentration at high temperature. These properties make CuO a promising material for solar cell applications as an absorbent layer and antireflection coating.

Keywords: CuO, TB-mBJ, GGA+U, Solar cells, Absorbent layer

Introduction

To achieve sustainable growth, the development of alternative energy sources to fossil fuels is critical. Solar energy, among these emerging energy sources, has become well-known and is rapidly expanding due to its ease of use, inexhaustibility, and environmental friendliness. The first efficient solar cell was created using a silicon p-n junction semiconductor, which is too costly for large-scale production. As a result, other light-absorbing materials that are low-cost, plentiful on the planet, and environmentally sustainable must be investigated. Semiconductor oxide solar cells are a viable alternative to silicon solar cells because they are less expensive to manufacture, non-toxic, and have a high light absorption rate. Transparent oxides (TCO) with a bandgap of about 3.4 eV, such as zinc oxide ZnO and tin dioxide TiO2, are well-known transparent oxides (TCO) that can absorb solar light only in the ultraviolet region of the solar spectrum. The semiconductor should have an optical band gap of 2 eV or less to better use solar energy. CuO and Cu_2O are TCOs with small band gaps of 1.35 eV [1] and 2.0 eV [2], respectively, corresponding to theoretical solar energy conversion efficiency of 31% [3,4] and 20% [5]. CuO and Cu_2O have slowly gained attention as a candidates for large-scale solar energy harvesting materials in recent years, with CuO dominating due to its smaller optical bandgap.

CuO can absorb the entire visible light spectrum, while Cu_2O can only absorb light with a wavelength less than 620 nm. CuO is therefore more stable in the air than Cu_2O, which can be oxidized to CuO for higher temperatures. When a CuO/ZnO barrier layer is used to monitor the carrier recombination dynamics in ZnO, Raksaet al. [6] reported improved performance in ZnO dye-sensitized solar cells (DSSCs). Lim et al. [7] reported a CuO/PCBM solar cell with a 0.04% performance. CuO's electronic structure has been successfully identified in the literature [8,9], demonstrating that CuO is intrinsically a p-type semiconductor and that n-type conduction in undoped CuO is impossible.

Besides, CuO is antiferromagnetic material with partial magnetic moments of 0.60 μ_B for the copper atoms and 0.14μ_B [10] for the oxygen atoms. It also presents a low resistivity at the average of 0.05 Ω.cm [11]. However, to identify CuO's intrinsic behavior for its application as an absorbing material in a photovoltaic cell, it is essential to perform density functional theory calculations (DFT) in atomistic scale. Several DFT studies in a variety of semiconductors have been reported, including ZnO[12-14] and GaN (gallium nitride) [15]. In this paper, we present first-principles DFT calculations of CuO using the Wien2K code and the Full Potential Linearized Augmented Plane Wave method (FP-LAPW). The LDA and GGA approximations of the Kohn-Sham density-functional theory with local and semi-local density approximations

have successfully predicted structural properties and cohesion energies, but the band gap value is underestimated. We used the two approximations DFT+U [17] and TB-mBJ[18] to resolve this problem and approximate the bandgap energy to its experimental value while retaining the appropriate structural parameters. The first method corrects the underestimated gap energy by incorporating the screened Coulomb interaction denoted by Hubbard term U into the potential of exchange and correlation, which avoids the excessive relocation of electrons in involved orbitals. The second one, recently developed by Tran and Blaha (TB-mBJ) [18], produces excellent improvements in the electronic, optical and electrical properties since it describes precisely the energies of d levels of metals.

1. Computational methods

In our calculations, we used the FP-LAPW method, which divides the space into two regions. The first region corresponds to the R_{MT} radius of muffin tin (MT) spheres, while the second corresponds to the interstitial space between the spheres. In the interstitial region, wave functions are formed in the radial part with spherical harmonics as a Schrödinger equation solution, and their energy derivatives and in-plane waves basis. The muffin tin radius values were optimized at 1.92 a.u. for copper atoms and 1.7 a.u. for oxygen atoms. The density of charge was Fourier-expanded up to G_{max}=14 au−1. The energy cutoff was optimized to be $K_{max} \times R_{MT}$=8, where Kmax is the maximum value of the reciprocal lattice vectors used in the plane waves expansion. These results were obtained with a convergence criterion of 10^{-5}Ry/unit cell. In our calculations, we treated Cu ($3d^{10}\ 4s^1$) and O ($2s^2\ 2p^4$) as valence states. The structural properties were investigated using a Perdew-Burke-Ernzerhof (GGA-PBEsol) approximation of the generalized gradient [19]. In addition, we used the GGA+U method for the electronic and optical properties, with U as the potential of Hubbard's orbital multi-average region, whose value is extracted from the experimental results to determine the XPS[20]. Also, and for comparison to the GGA+U method, we opted for the modified Becke-Johnson (TB-mBJ) potential, a modified version of the Becke and Johnson functional[21]. The following formula expresses the TB-mBJ potential:

$$v_{x,\sigma}^{MBJ}(r) = c\,v_{x,\sigma}^{BR}(r) + (3c-2)/\pi\,\sqrt{5/12}\,\sqrt{2\,t_\sigma(r)/\rho_\sigma(r)} \qquad (1)$$

<div style="text-align:right">(1)</div>

where $\rho_\sigma(r)=\sum_{i=1}^{N_\sigma}\left|\Psi_{i\sigma}\right|^2$, $t_\sigma(r)=\frac{1}{2}\sum_{i=1}^{N_\sigma}\left|\Psi_{i\sigma}^{\dot{c}}\nabla\Psi_{i\sigma}\right|^2$ and $v_{x,\sigma}^{BR}(r)$ are the electron density, the density of

kinetic energy, and the Becke Roussel (BR) potential[22], respectively.

The main modification is at the level of the parameter c in the formula of the functional. This

parameter was chosen to depend linearly on the square root of the average $\dfrac{\left|\nabla\rho(r)\right|}{\rho(r)}$ which is

given by:

$$c=\alpha+\beta\dot{c}\dot{c}(2)$$

where α=-0.012 Bohr$^{1/2}$, β=1.023 Bohr$^{1/2}$ are constant and V_{cell} is the volume of the unit cell.

The optical properties are determined using the knowledge of the dielectric function $\varepsilon(\omega)$ that

consists of a real part $\varepsilon_1(\omega)$ and an imaginary part $\varepsilon_2(\omega)$, given by:

$$\varepsilon(\omega)=\varepsilon_1(\omega)+i\varepsilon_2(\omega)(3)$$

The real and the imaginary part are expressed through the following formula[23,24]:

$$\varepsilon_2(\omega)=\dot{c}\dot{c}(4)$$

$$\varepsilon_1(\omega)=1+\dot{c}\dot{c} \qquad\qquad (5)$$

where $M_{nn'}(k)$ denotes the dipole matrices components, $\omega_{nn'(k)}$ denotes the energy difference

between the initial and final states, S_k represents the surface energy, and P denotes the principal

value of the integral.

Other important optical properties, such as the absorption coefficient, reflectivity, and transmitt

ance, can be estimated using the imaginary dielectric function. The absorption coefficient

$\alpha(\omega)$, refractive index $n(\omega)$, the reflectivity $R(\omega)$, the loss energy function L(ω) and optical

conductivity $\boldsymbol{\sigma}(\omega)$ are calculated using these formulas [25]:

$$\alpha(\omega)=\sqrt{2}\omega\left[\left[\varepsilon_1^2(\omega)+\varepsilon_2^2(\omega)\right]\dot{c}\dot{c}1/2-\varepsilon_1(\omega)\right]^{1/2}\dot{c}(6)$$

$$n(\omega)=\frac{1}{\sqrt{2}}\left[\left[\varepsilon_1^2(\omega)+\varepsilon_2^2(\omega)\right]\dot{c}\dot{c}1/2+\varepsilon_1(\omega)\right]^{1/2}\dot{c} \qquad (7)$$

$$R(\omega)=\lceil(\varepsilon(\omega)-1)^{1/2}/(\varepsilon(\omega)+1)^{1/2}\rceil^2(8)$$

$$L(\omega)=-\Im 1/\varepsilon=\varepsilon_2(\omega)/(\varepsilon_1(\omega)+\varepsilon_2(\omega))^2(9)$$

4

$$\Re(\sigma(\omega))=\omega/4\pi\Im(\varepsilon(\omega))\quad(10)$$

The transmittance $T(\omega)$ was calculated using the following formula [26], where d is the thickness of the structure.

$$T(\omega)=(1-R(\omega))^2\,exp(-\alpha d)\quad(11)$$

2. Results and Discussion

2.1 Structural Properties

CuO crystallizes in the monoclinic C2/c space group [23]. Fig.1 shows the unit cell of CuO used in this study. This structure was obtained from a monoclinic unit cell formed by four atoms where Cu occupied the positions (1/4, 1/2, 3/4) and (3/4, 0, 3/4), whereas O occupied the sites (0, 1/4, 0,417) and (0, 3/4, 0,583).
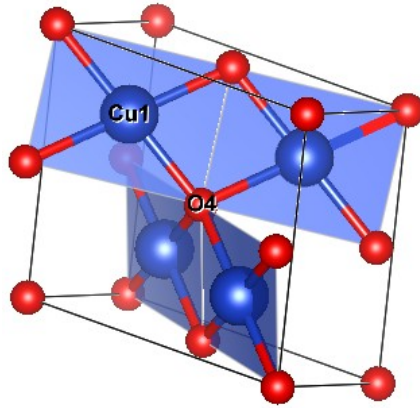

Fig. 1: Unit cell of CuO with the oxygen and the copper atoms represented respectively by the red and the blue atoms.

To find the equilibrium state, the CuO's structural parameters were optimized using a 4D-optimize package available in the Wien2k code, which minimizes four parameters according to the most stable antiferromagnetic state our case: the lattice parameters a, b, c, and the angle γ simultaneously. The values of these parameters are represented in table 1 and compared to the experimental values and the other results of calculations. Our results are in agreement with the other theoretical and experimental data.

Table 1.Theoretical and experimental structural parameters of CuO

Structure parameters	Our work	Other calculations	Experiments
a	3.428	3.48 [27] - 3.44 [23]	3.422 [29] - 3.429 [25]

b	4.683	4.76 [27] - 4.55 [23]	4.683 [29] - 4.692 [25]
c	5.134	5.21 [27] - 4.99 [28]	5.128 [29] - 5.137 [25]
γ	99.560	99.5 [27,28]	99.5 [29,30]
bond length Cu-O	2.4629	2.4655[26],2.45[27]	2.464[29]-2.466[30]

A way of studying the structural properties is to display the spectrum of X-ray diffraction (XRD). Fig.2(a) shows the simulated XRD spectrum of CuO for optimized structure using the VESTA code [31]. CuO is polycrystalline, has a monoclinic system, and has (111), (-111), and (112) peaks, according to the spectra.

The strongest peak is (111), indicating that this is the preferred growth orientation in bulk CuO, which is consistent with experimental data [30-32]. To check the thermodynamic stability we have also calculated the phonon density of states and phonon band. As shown in Fig.2(b) all the bands are above 0 meV in positive range confirms its structural stability and supports room temperature fabrication. We have observed a strong electron-phonon coupling in 0-18 meV with lowering of optical branches and mixing with acoustic branches.
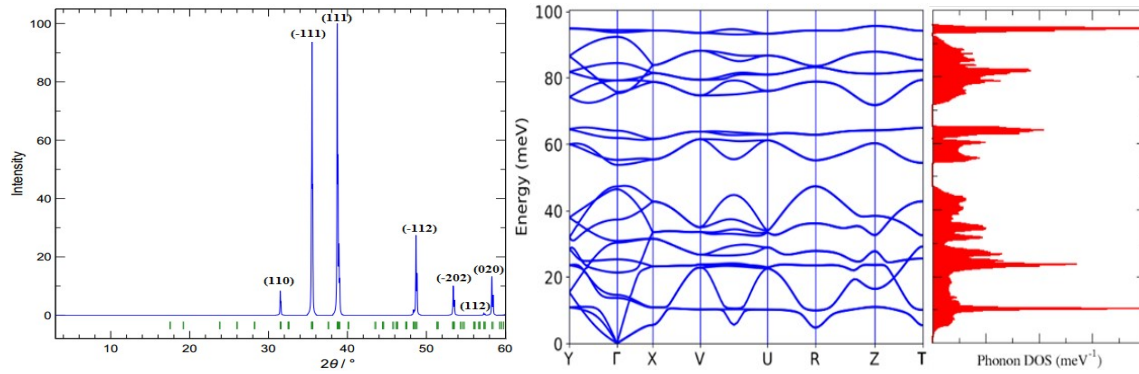

Fig. 2: (a) SimulatedX-Rays Diffraction spectrum for the optimized structure of CuO (b) Phonon band and density of state (Phonon-dos).

2.2 Electronic Properties:

2.2.1 Density of states and bands structure

Understanding the electronic structure of a material requires the study of the band structure, the partial and total density of states (PDOS and TDOS), which will allow us to analyze the

electronic character of the system. For that reason, we calculated the PDOS, TDOS, and the band structure of CuO for the optimized structure using the two approximations GGA+U with U=7.14eV and TB-mBJ. The Fermi level is taken as the origin of the energies. By examining the total density of states for both up and down states from GGA+U and TB-mBJ, we can see CuO's antiferromagnetic character [see Fig.3]. Indeed the two states are symmetric with a partial magnetic moment of 0.68 μ_B for the copper atoms and 0.09μB for the oxygen atoms. By analyzing the Partial DOS of CuO in this figure, we note that the valence band's deepest states are mostly dominated by the orbital O-2s located between-19.41eV and -17.27 eV for GGA+U and between -19.5eV and -17.5eV for the TB-mBJ approximation. The top of the valence band is dominated by the 3d orbital of the copper cations and the 2p orbital of the oxygen anions. Meanwhile, the states of these orbitals are located at the intervals [-8.17eV, 0eV] for GGA+U and [-8.5eV, 0eV] for the TB-mBJ. We can also see the O-2p and Cu-3d orbitals' significant hybridization around -5.1eV for GGA+U and -5.5eV for TB-mBJ. Concerning the conduction band, there is a low contribution of O-2p states located at [1.58eV,10eV] for the GGA+U and [2.06eV, 10eV] for the TB-mBJ as well as a low contribution of 4s and 2s states respectively of copper and oxygen. These results are in good conformity with the experimental and theoretical data [29,30,32].
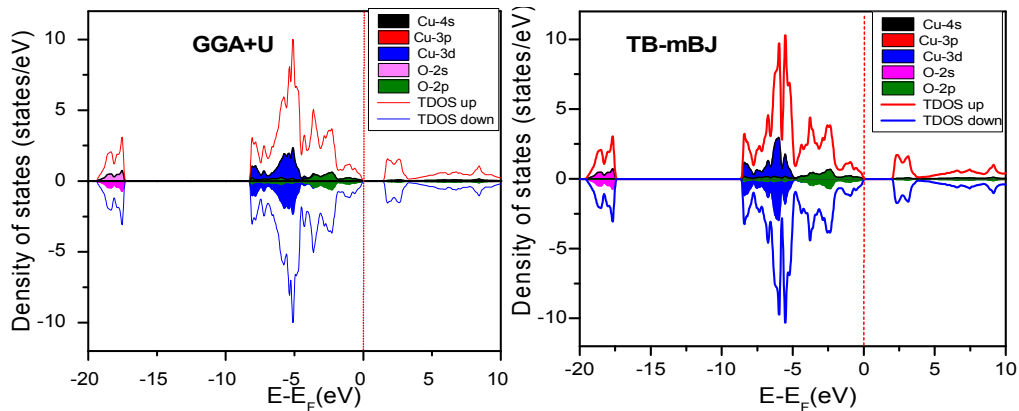

Fig. 3: Up and down Partial and Total Density of States of CuO calculated with GGA+U and TB-mBJ

The band structures presented in Fig.4 using GGA+U and TB-mBJ methods show that CuO is a direct bandgap semiconductor since the maximum of the valence band and the minimum of the conduction band are situated in the same point gamma. Moreover, it seems that states above the Fermi level at gamma point justifies that CuO is intrinsically a p-type as reported experimentally [32]. We also note that the modification brought by the TB-mBJ appears in the

shift of the bandgap energy seen the good description of the correlation between the O-2p and Cu-3d orbitals in this approximation compared to the GGA+U method.
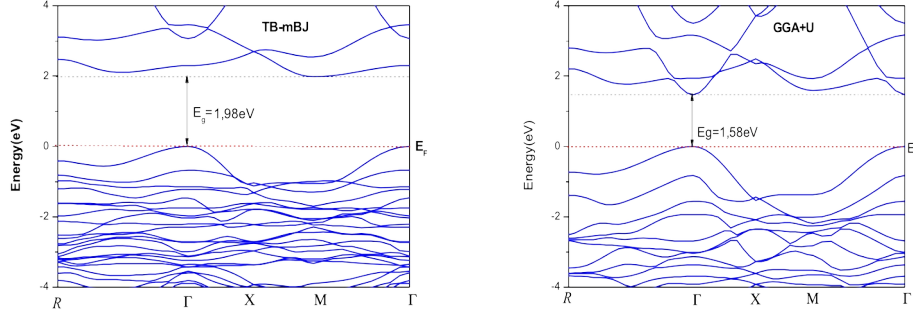

Fig. 4: Band structure of CuO calculated by both methods GGA+U and TB-mBJ

The bandgap values calculated by both the methods compared to other experimental and theoretical results are listed in table 2. The values obtained by the TB-mBJ approximation are in good conformity with the experimental data [30,32,33].

Table 2.Calculated band gap of CuO compared to experimental and other theoretical data

Our work	Experimental	Other calculations
2.02 eV (TB-mBJ) 1.577 eV (GGA+U)	2.1eV [29,30,32]	1.25 eV (GGA+U) [34] 1eV (LDA+U) [35] 1.21 eV (LDA+U) [27] 1.3 eV (GGA+U) [27]

2.2.2 Electron density

To understand the nature of the interactions between atoms in the CuO structure, we calculated the electron charge density distributions. Fig.5 shows the charge density distribution in the (111) CuO plane around the two nuclei of copper and oxygen atoms. The charge density contours provide information on the type of bond between the two atoms.
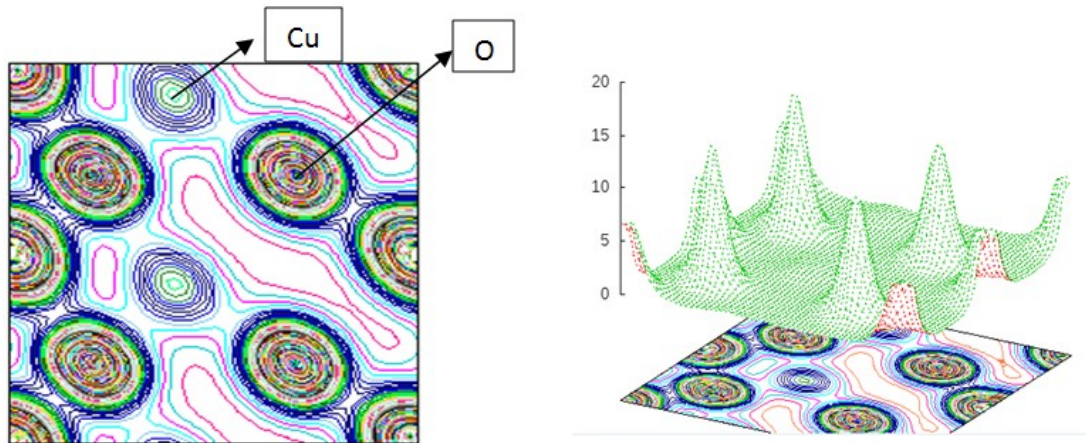
Fig. 5: Contours of CuO density of charge in the (111) plane

From this figure, we notice polarized electronic clouds in the charge repartition between the two atoms Cu and O, predicting mixed covalent and ionic bonds of Cu-O. The partial covalent behavior is due to the hybridization of Cu-3d with O-2p states in the valence band near the Fermi energy level. While the partial ionic character is due to the O atom's high electronegativity, which leads to appearing a bump in the electron charge density of oxygen and makes this atom acts as the center of charge accumulation.

2.3 Optical Properties:

The FP-LAPW is an excellent theoretical approach integrated in computation for calculating a compound's optical properties. These properties provide useful details about the compound's internal structure. The optical parameters like the real part of dielectric function $\varepsilon_1(\omega)$, the imaginary part of dielectric function $\varepsilon_2(\omega)$, the reflectivity $R(\omega)$, the energy electron loss function (EELS) $L(\omega)$, the refractive index $n(\omega)$ and the optical conductivity $\boldsymbol{\sigma}(\omega)$ of CuO were calculated in the range of photon energy 0-30 eV using GGA+U and TB-mBJ approximations. All the results of optical properties are shown in Fig.6(a-e). It appears from Fig.6(a) that the absorption threshold (first critical point) of the imaginary dielectric function occurs at energies 1.8eV and 2.4 eV for GGA+U and TB-mBJ, respectively. These energies give the threshold of the direct optical transitions between the highest of the valence band and the lowest state of the conduction band. This is known as the fundamental absorption threshold, the origin of these peaks attributed to the partial density of states. The interband transitions between the p-states of the O atoms to the 4s states of the Cu atoms lead to an absorption peak. Beyond these energies, we can notice a rapid increase in $\varepsilon_2(\omega)$ since the number of critical transitions contributing to $\varepsilon_2(\omega)$ increases abruptly. For the real part of the

9

dielectric function $\varepsilon_1(\omega)$ [Fig.6(b)], the most important quantity is the static limit $\varepsilon_1(0)$ which allows us to calculate the refractive index at the static limit. This value is $\varepsilon_1(0) = 5.18$in the GGA+U and $\varepsilon_1(0) = 3.48$ in TB-mBJ. This real part begins to increase to the peaks at about 1.8 eV and 2.4 eV, respectively, calculated by adopting the two approximations GGA+U and TB-mBJ. It begins to increase and reaches the maximum value at 2.74 eV(GGA+U) and 3.45 eV(TB-mBJ). After reaching 18.58eV using GGA+U and 19.34 eV with TB-mBJ, it starts to decrease further below zero in negative scale for the ranges respectively 20.45–25.26 eV and 20.93–25.34 eV. The difference in the calculated results from the TB-mBJ and the GGA+U is justified by the small shift between the band gap's values. CuO shows a metallic behavior at the negative values of real dielectric function $\varepsilon_1(\omega)$; otherwise, it is dielectric. Concerning the optical reflectivity $R(\omega)$ as shown in Fig.6(c), the zero-frequency reflectivity is about 15% and 9% from GGA+U and TB-mBJ, respectively. The material is transparent due to its low reflectivity in the infrared and visible energy ranges. In this part of the energy spectrum, it can thus be used as an anti-reflective coating material. At 24 eV and 24.5 eV, respectively, GGA+U and TB-mBJ have maximum reflectivity values of about 35% and 37%. Interestingly, the maximum reflectivity occurs when the real part of dielectric function $\varepsilon_1(\omega)$ goes below zero, as seen from Fig.6(a). In general, the reflectivity indicates a decrease at the plasma frequency ω_p. This frequency is linearly correlated to the electronic density of the material. In metals, the densities are such that the frequency of the plasma ω_p tumbles into the highly visible or ultraviolet range. When $\omega < \omega_p$, in the high-frequency region, the real dielectric function becomes negative, $\varepsilon_1(\omega) < 0$.

Consequently, we obtain the maximum reflectivity $R(\omega)$ when the real dielectric function is less than zero. The EELS function is an essential factor that describes the energy loss of a fast electron that passes through the material. The EELS function $L(\omega)$presented in Fig.6(d) shows low-intensity peaks at low energies corresponding to transitions from the valence band to the conduction band. The higher peak occurring at energies 25.73eV and 25.56eV for respectively GGA+U and TB-mBJ approximations is defined as the energy ($\hbar\omega_p$) of massive plasmons that occurs as seen below when the imaginary part of the dielectric function is less than 1. The real part is zero, correspondings to the abrupt reduction of the optimal intensity of the reflectivity and the transition of CuO between the metallic and dielectric behavior justified by the sign transition of the real dielectric function. These calculated plasmons energies are in agreement with the experimental value [35].
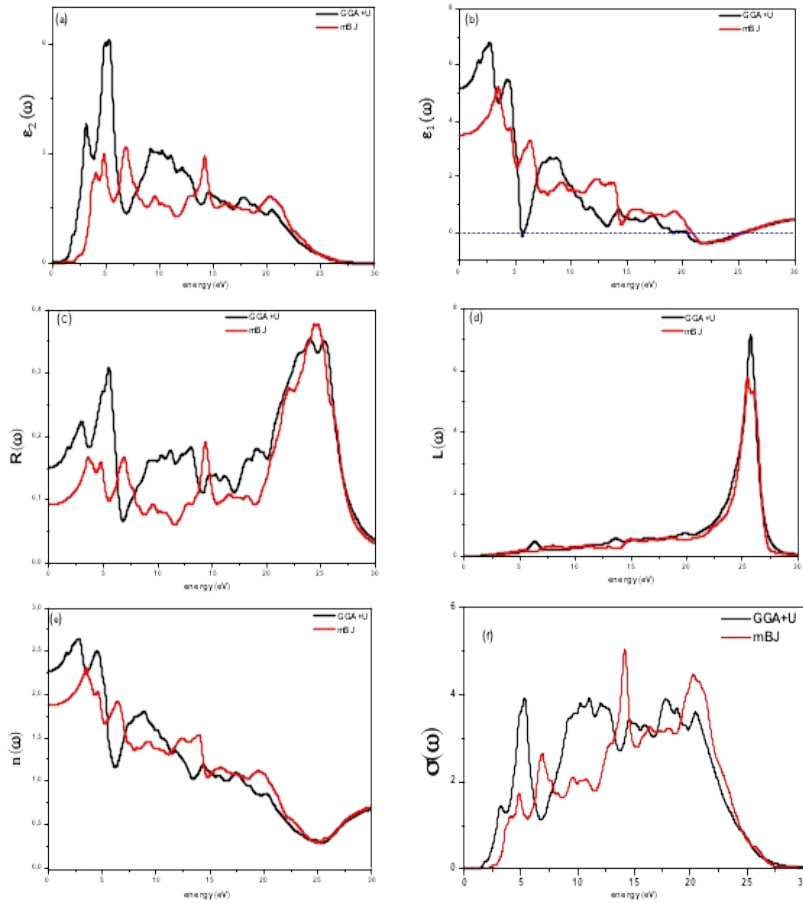
Fig. 6: Optical spectra as a function of photon energy for CuO : (a) imaginary and (b) real parts of dielectric function, (c) reflectivity, (d) energy loss function, (e) refractive index and (f) optical conductivity.

By analyzing figure 6(e), it is found that the static refractive index n(0) of CuO to have the value 2.28 and 1.89 respectively for GGA+U and TB-mBJ. Using the GGA+U and TB-mBJ approaches, the refractive index increases as the frequency increases, reaching an average value of 2.33 and 1.97 in the visible range, respectively. Since photons are delayed when they penetrate a substance due to interactions with electrons, the refractive index is greater than one. The more the refractive index is, the more the photons are slowed by browsing a material. It appears by analyzing Fig.6(f) that the optical conductivity of CuO begins from the energies of about 1.58 and 2.03eV, respectively, using both approximations GGA+U and TB-mBJ. These values represent the optical band gap to overcome for the beginning of the electronic transition. This optical conductivity begins to increase from this energy value and reaches a maximum level located near the visible range, making the CuO an excellent candidate to be used in photovoltaic applications. The presence of intensity of absorption and the transmittance spectra

in the visible range predict its application as an absorbent layer in the solar cells [Fig.7(a,b)]. CuO offers a strong absorption below 400 nm due to electrons' transition from the O-2p orbitals (valence-band) to Cu-4s orbital (conduction-band). Usually, this value of wavelength is referred to as the bandgap. We can add that this absorption decreases in the visible and IR regions and stays about $10^4 cm^{-1}$. The transmittance spectrum presents a conversely proportional character to the absorption coefficient. For this reason, it is clear that the transmittance spectra of CuO present an average transmittance of the order of 60 % to 67 % between800 nm and 1000 nm, respectively, using the GGA+U and the TB-mBJmethods. The abrupt drop of the transmittance for the wavelength lower than 700 nm corresponds to the absorption in the copper oxide owed to the electronic transitions between the valence band and the conduction band. In the low wavelengths <380 nm, the values of the transmittance of CuO are close to 0%. We also notice that the transmittance spectrum covers an extensive range of light using TB-mBJ approximation, which is related to the shift of gap energy as reported below and shown in Fig.7(b), illustrating the optical band gap calculated using GGA+U and TB-mBJ.These curves are in perfect coherence with the results obtained from the experimental results [32,34,36,37]. The optical band gap has been determined by using the Tauc formula [38] given by:

$$(\alpha h v)^2 = B(hv - E_g) \qquad\qquad (12)$$

where B is a constant, ($hv¿$is the energy of the incident photon, and α is the absorption coefficient. By plotting $(\alpha h v)^2$ according to $(h v)$ and by the extrapolation until$(\alpha h v)^2=0$, we can determine the optical bandgap's value, which is shown in Fig.7(b). We conclude that the bandgap values deducted by the relation of Tauc are 1.803 eV and 2.596 eV using GGA+U and TB-mBJ approaches, respectively. These results are in good agreement with the experimental values 2.64 deduced by Ibrahim Y. Erdo et al.[38], and 2.55 eV reported by R. Shabu et al. [32]. One way to justify the use of CuO as an absorber window of the solar cells is to evaluate the quantum efficiency, maximum absorption of these structures, and the maximum photocurrent generated as a function of the layer's thickness. For this reason, we evaluate these parameters, which are calculated using lighting with the AM 1.5 G spectrum. The bandgap of CuO leads to an improvement of the absorption. It is very well that these structures can be considered as absorbers for films with significant thicknesses. We also notice that this absorption in the visible is at the origin to generate a photocurrent maximum of 8 mA/cm2. These results open the horizon of using this material as transparent windows in solar cells.

Fig. 7: (a) Absorption Coefficient and transmittance, (b) Optical band gap of CuO calculated with GGA+U and TB-mBJ approximations.
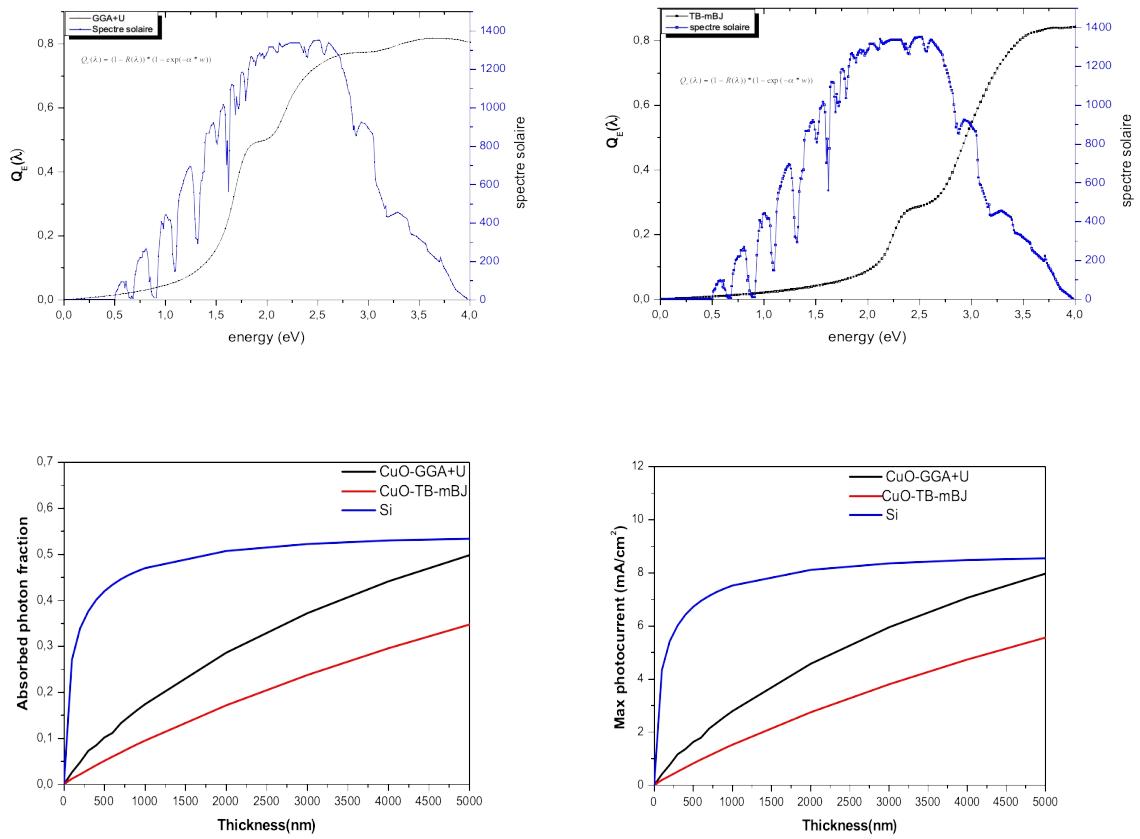

Fig.8: quantum efficieny, absorbed photon and maximum photocurrent of CuO calculated using TB-mBJ method.

2.3 Electrical Properties:

Electrical properties present a critical aspect of the performance of the materials. For this reason, we have calculated the electrical conductivity using the Boltztrap code [39]. This is based on the semi-classical Boltzmann theory. This package uses the calculated electronic structure data obtained from Wien2K. The integration of the Boltzmann distribution gets electrical conductivity. This formula is a function of the temperature and the chemical potential via the following equation:
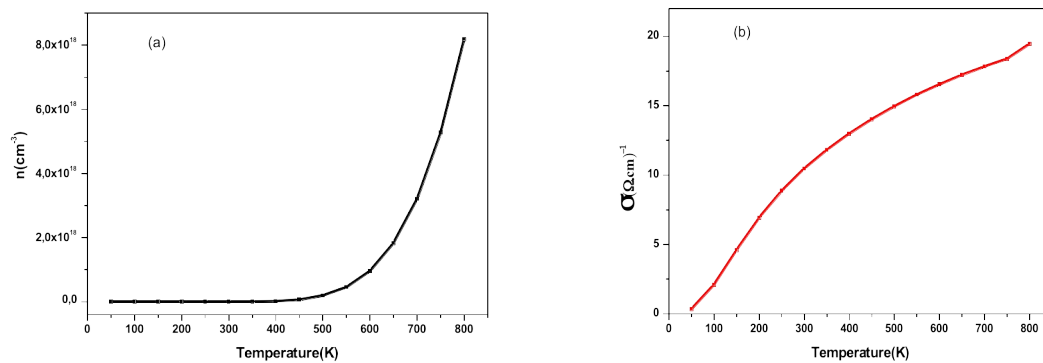
$$\sigma_{\alpha\beta}(T,\mu)=(1¿¿\Omega)\int \sigma_{\alpha\beta}(\epsilon)\left[-\partial f_{\mu}(T,\epsilon)/\partial \epsilon\right]d\epsilon \; ¿(13)$$

Where α,β denote the tensor indices, Ω, f_{μ}, T and μ are the unit cell volume, the Fermi distribution function, the temperature, and the chemical potential. However, the semi-classical Boltzman theory is remaining unable to determine the scattering rate. To overcome this difficulty, we used the model suggested by Ong et al. [40], who estimated the relaxation time by relationship:

$$\tau=2.53\,10^{-5}T^{-1}n^{-1/3}(14)$$

where τ is expressed in second in Kelvin and n is the electron concentration in cm^{-3}.

The electrical conductivity, carrier density and carrier mobility are shown in Fig.8 as a temperature function. We can see that as the temperature rises, the carrier concentration and conductivity rise, while the carrier mobility rises and then falls, reaching a limit at 220K. These findings point to the formation of thermal agitation in free carriers as they move from the valence band to the conduction band. Also, it is shown that the conductivity variation of CuO is limited at low temperature (T<250K) by the interpretation of the carrier mobility. Above 350K, the conductivity is primarily defined by the carrier concentration, which suggests CuO's semiconductor behavior. These findings are consistent with experimental results [11,32].
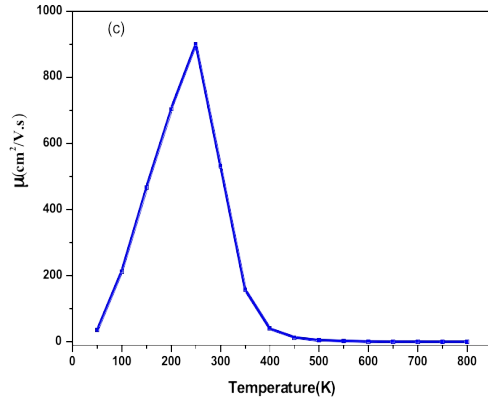

14

Fig. 8 (a) Carrier concentration, (b) Electrical conductivity and (c) Carrier mobility of CuO as a function of temperature

Conclusion

  The structural, mechanical, optical, and electrical properties of the CuO monoclinic structure were investigated in this paper. The GGA-PBEsol approximation was used to measure the structural properties. The PBEsol accurately represented the structural properties but underestimated the band gap value, according to our findings. Electronic, optical, and electrical properties are investigated using GGA+U and TB-mBJ potential to resolve this problem. We discovered that the latter method, which relies based on modified Becke-Johnson potential with kinetic energy density approximation, provides a high level of accuracy that matches experimental data. According to its electronic and optical properties, CuO has a direct bandgap between 1.58 and 2.03 eV and a low transmittance in visible light, which justifies its strongest domains of activity as an absorbent layer in visible light. CuO appears to have semiconductor behavior, with electrical conductivity controlled by carrier charge mobility and concentration, based on its electrical properties.

References

[1] F. Marabelli, G. B. Parravicini, and F. Salghetti-Drioli, Phys. Rev. B52,1433 (1995).

[2] T. V. Pham, M. Rao, P. Andreasson, Y. Peng, and J. Wang, Appl. Phys. Lett.102, 032101 (2013).

15

[3] W. Shockley and H. J. Queisser, J. Appl. Phys. 32(3), 510 (1961).

[4] M. C. Hanna and A. J. Nozik, J. Appl. Phys.100(7), 074510 (2006).

[5] A. Mittiga, E. Salza, F. Sarto, M. Tucci, and R. Vasanthi, Appl. Phys. Lett.88, 163502 (2006).

[6] P.Raksa, S.Nilphai,A.Gardchareon,andS.Choopun, Thin Solid Films 517, 4741– 4744(2009).

[7] Y.-F.Lim, J.J. Choi, and T.Hanrath, J. Nanomater.2012, 393160 (2012).

[8] D. Wu, Q. Zhang, and M. Tao, Phys. Rev. B73, 235206 (2006).

[9] M. Nolan and Simon D. Elliott, Phys. Chem. Chem. Phys.8, 5350 (2006).

[10] J. B. Forsyth, P. J. Brown, and B. M. Wanklyn, J. Phys. C21, 2917 (1988).

[11] D. Gopalakrishna, et al, Ceramics International 39, 7685-7691(2013).

[12] E.-C. Lee and K. J. Chang, Phys. Rev. B70, 115210(2004).

[13] Y. Yan, M. M. Al-Jassim, and S.-H.Wei, Appl. Phys. Lett.89, 181912 (2006).

[14] Z. G. Yu, H. Gong, and P. Wu, Chem. Mater.17, 852 (2005).

[15] J. Neugebauer and Chris G. Van de Walle, J.Appl. Phys. 85, 3003 (1999).

[16] Perdew J P, Burke K and Ernzerhof M. Phys. Rev. Lett. 77 3865, (1996).

[17] S.L.Dudarev,G.A. Botton, S.Y. Savarsov, C.J. Humphreys, A.P. Sutton, Phys. Rev.B 57, 1505 (1998).

[18] F. Tran, P. Blaha, Phys. Rev. Lett. 102, 226401(2009).

[19] John P. Perdew, and al., Phys. Rev. Lett. 100, 136406 (2008)

[20] A.Fujimori,PhysRevB28(8),4489-4499(1983).

[21] A. D. Becke and E. R. Johnson, J. Chem. Phys. 124, 221101(2006).

[22]A. D. Becke and M. R. Roussel, Phys. Rev. A 39, 3761 (1989).

[23] J. Sun, H.Wang, J. He, Y. Tian, Phys. Rev. B71, 123132(2005).

[24] F. Wooten, Optical Properties of Solids Academic, New York, (1972).

[25] H. Lashgari et al. Applied Surface Science 369, 76–81(2016).

[26] E. F. Keskenler, S. Dogan, B. Diyarbakir, S. Duman, and B. Guurbulak, J. Sol-Gel Sci. Technol. 60, 66–70 (2011).

[27] Vincent Oison and all, surface Surface Science 622, 44–50(2014).

[28] D. Wu, Q. Zhang, M. Tao, Phys. Rev. B 73, 235206(2006).

[29] ICSD, Inorganic Crystal Structure Database (ICSD), National Institute of Standards and Technology (NIST) Release 2013/1, vol. 1 (2013).

[30] R. Shabu, and al, Materials Research Bulletin 68, 18(2015).

[31]K. Momma and F. Izumi, "VESTA 3 for three-dimensional visualization of crystal, volumetric and morphology data," J. Appl. Crystallogr. 1272-1276, 1272-1276(2011).

[32] G. Papadimitropoulos, N. Vourdas, V.Em. Vamvakas, D. Davazoglou, Thin Solid Films 515, 2428– 2432(2006).

[33] A. Tombak et al. Results in Physics 5, 314–321(2015).

[34] C.E. Ekuma, V.I. Anisimov, J. Moreno, and M. Jarrell, Eur. Phys. J. B, 87: 23(2014).

[35]Dangxin Wu, Qiming Zhang, and Meng Tao, Phys. Rev. B 73, 235206(2006).

[36]D Tahir and S Tougaard, J. Phys. Condens.Matter 24, 175002(2012).

[37] A. David, N.F. Mott, Philos. Mag. 22, 903(1970).

[38] Ibrahim Y. Erdo and all, Journal of Alloys and Compounds 492, 378–383(2010).

[39] G.K.H. Madsen, D.J. Singh, Comput. Phys. Commun. 175, 67(2006).

[40]Khuong P Ong, David J. Singh, and Ping Wu, physical review B 83,115110(2011).